

1
2 **Visualizing formation and dynamics of a three-dimensional sponge-like network**
3 **of a coacervate in real time**
4

5 Ryou Kubota^{1,*}, Taro Hiroi^{1,‡}, Yuchong Liu^{1,‡}, Itaru Hamachi^{1,2,*}

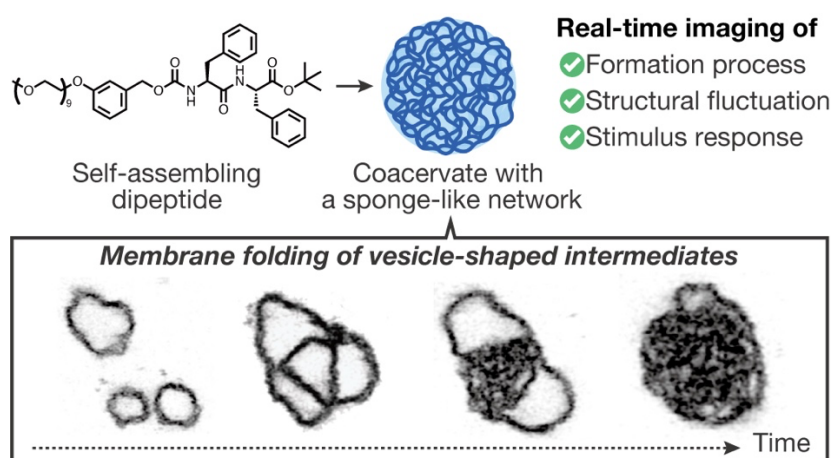
6
7 ¹Department of Synthetic Chemistry and Biological Chemistry, Graduate School of Engineering,
8 Kyoto University, Katsura, Nishikyo-ku, Kyoto 615-8510, Japan

9 ²JST-ERATO, Hamachi Innovative Molecular Technology for Neuroscience, Kyoto University,
10 Katsura, Nishikyo-ku, 615-8530, Japan.

11 [‡]These authors contributed equally to this work

12
13 Correspondence to: rkubota@sbchem.kyoto-u.ac.jp, ihamachi@sbchem.kyoto-u.ac.jp

14
15
16 **Graphical abstract**



1 **Abstract**

2 Coacervates, which are formed by liquid–liquid phase separation, have been extensively explored as
3 models for synthetic cells and membraneless organelles, so their in-depth structural analysis is
4 crucial. However, both the inner structure dynamics and formation mechanism of coacervates
5 remain elusive. Herein, we demonstrate real-time confocal observation of a three-dimensional
6 sponge-like network in a dipeptide-based coacervate. *In situ* generation of the dipeptide allowed us
7 to capture the emergence of the sponge-like network via unprecedented membrane folding of
8 vesicle-shaped intermediates. We also visualized dynamic fluctuation of the network, including
9 reversible engagement/disengagement of crosslinks and a stochastic network kissing event. Photo-
10 induced transient formation of a multiphase coacervate was achieved with a thermally responsive
11 phase transition. Our findings expand the fundamental understanding of synthetic and biological
12 coacervates, and provide opportunities to manipulate their physicochemical properties by
13 engineering the inner network for potential applications in life-like material fabrication and
14 biomedical research.

15 16 **Introduction**

17 A coacervate is a condensed fluid that forms by the liquid–liquid phase separation (LLPS) of small
18 organic molecules, polypeptides, pairs of oppositely charged polyelectrolytes, or
19 biomacromolecules in aqueous solution.^{1–8} Coacervates are highly dynamic. They exhibit a variety
20 of unique behaviors, including coalescence into larger spherical assemblies upon contact with one
21 another; facilitated chemical reactions upon internal molecular sequestration; and metastability by
22 transforming into solid-like amyloid fibrils. Owing to their distinctive behavior, coacervates have
23 long been recognized as attractive models for protocells and artificial cells in research into the
24 origins of life.^{9–19} In the field of cell biology, biomolecular liquid-like condensates have emerged as
25 a new aspect of intracellular compartmentalization. They are increasingly considered to play
26 important roles in a plethora of biological functions and neurological disorders involving amyloid
27 fibrils through spatiotemporally controlled formation/dissolution.²⁰

28 In-depth analysis of the inner structure of a coacervate and its dynamics is essential for
29 understanding synthetic and biological coacervate systems and their application. Therefore,
30 extensive efforts have been made in this field. Cryogenic transmission/scanning electron
31 microscopy (cryo-TEM/SEM) has been used to visualize three-dimensional (3D) sponge-like
32 bicontinuous networks, which are composed of condensed molecules and aqueous phases, and
33 constitute the inner structures of a wide range of synthetic coacervates.^{21–27} In 1990, Bassereau *et al.*

1 reported a randomly connected bilayer network in a coacervate composed of cetylpyridinium
2 chloride and 1-hexanol by freeze-fracture electron microscopy (EM).²² Kataoka, Kishimura *et al.*
3 demonstrated TEM tomographic images of the 3D connected network comprising unilamellar
4 membranes in a polyethylene glycol (PEG)-modified polyelectrolyte complex fixed with
5 glutaraldehyde.²⁶ These 3D sponge-like network structures may be consistent with structural density
6 fluctuation detected by small-angle X-ray/neutron scattering measurements, by which the averaged
7 mesh size was estimated to be 1–100 nm.^{28–30} However, EM inevitably requires drying, freezing,
8 and/or fixation for sample preparation, so that only static images of the specimens can be illustrated,
9 and dynamic information about the sponge-like network is not clearly addressed. Although time-
10 lapse observation of coacervates is widely conducted by widefield and confocal microscopy,³¹ to
11 date these light-based imaging techniques have visualized only homogeneous structures of
12 coacervates, but not yet sponge-like morphologies. Moreover, it is generally considered that
13 coacervates form through nucleation or spinodal decomposition.^{32,33} The formation mechanism of a
14 sponge-like morphology has never been examined by microscopic or spectroscopic methods.
15 Therefore, both the inner structure dynamics and the formation mechanism of 3D sponge-like
16 networks remain elusive.

17 Herein, we describe real-time imaging of the generation and dynamics of a 3D sponge-like
18 network in a dipeptide-based coacervate by confocal-based super-resolution microscopy (Fig. 1a). A
19 diphenylalanine peptide modified with a *tert*-butyl ester at the *C*-terminus (FF-OtBu; F = L-
20 phenylalanine) was recently developed as a novel structural motif for LLPS.³⁴ To examine its
21 formation process in real time, we designed a reaction for *in situ* generation of the FF-OtBu core, in
22 which two distinct phenylalanine fragments were linked to yield a coacervate-forming dipeptide
23 (PEG₉-FF-OtBu, Fig. 1b). Time-lapse imaging reveals the emergence of a 3D sponge-like network
24 in a coacervate, which proceeds through the unexpected membrane folding of vesicle-shaped
25 intermediates. The resulting interpenetrated network exhibits dynamic structural fluctuation, which
26 has not yet been investigated by EM; i.e., the spontaneous engagement and disengagement of
27 network crosslinks, and a stochastic kissing event between the outer networks of different
28 coacervate droplets before fusion. Furthermore, we succeeded in demonstrating a pathway-
29 dependent thermally responsive phase transition, in which the intermediate states differed
30 depending on temperature. The transient generation of a multiphase coacervate can also be achieved
31 by the local irradiation of gold nanoparticles encapsulated in a coacervate with a laser.

32

1 **Results**

2 **Real-time imaging of the coacervate formation process via *in situ* synthesis**

3 We recently discovered FF-OtBu, which is a structurally simple motif for LLPS. We modified an
4 FF dipeptide that has often been used as a self-assembling moiety^{4,35-38} with a bulky *t*-Bu group at
5 the *C*-terminus to suppress the formation of supramolecular nanofibers via steric hindrance
6 (Supplementary Fig. 1). Our objective was to induce LLPS. We demonstrated that the resultant
7 coacervate enabled molecular sequestration and facilitated internal reactions.³⁴ In the present study,
8 we generated an FF-OtBu motif by condensing an *N*-terminus-modified phenylalanine (*N*-modified
9 F-OH) and a phenylalaninate *tert*-butyl ester (H-F-OtBu) *in situ* in an aqueous buffer solution to
10 investigate the formation of a coacervate in real time (Fig. 2a). It was expected that as the reaction
11 progressed, the concentration of the FF-OtBu derivative would gradually increase and exceed the
12 critical concentration, thereby enabling the aggregate formation process to be observed *in situ* in
13 real time. We used a phenylalanine derivative modified with a hydrophilic nonaethylene glycol
14 group at the *N*-terminus (PEG₉-F-OH). DMT-MM (4-(4,6-dimethoxy-1,3,5-triazin-2-yl)-4-
15 methylmorpholinium chloride) was selected as a condensation reagent because of the higher
16 reactivity under mild aqueous conditions than 1-ethyl-3-(3-dimethylaminopropyl)carbodiimide
17 (EDC; another water-soluble condensation reagent) and its water-soluble side-products that may not
18 interfere with self-assembly.³⁹ The reaction was initiated by adding a buffer solution comprising
19 DMT-MM to a mixture of PEG₉-F-OH and H-F-OtBu, and incubating the mixture at 25 °C. The
20 transmittance gradually decreased as the reaction proceeded, indicating that certain self-assemblies
21 had formed (Supplementary Fig. 2). Reverse-phase high-performance liquid chromatography (RP-
22 HPLC) analysis of the reaction mixture confirmed the formation of the desired product, i.e., PEG₉-
23 FF-OtBu (Supplementary Fig. 3).

24 We next monitored the formation of self-assemblies comprising PEG₉-FF-OtBu by confocal-
25 based super-resolution Airyscan imaging in real time. We used a hydrophobic rhodamine 6G
26 (rho6G) dye as a fluorescent probe (Supplementary Fig. 1). Time-lapse imaging revealed the unique
27 formation of coacervate droplets via the membrane folding of vesicle-like assemblies as key
28 intermediates (Fig. 2b, Supplementary Movie 1). No structures were observed during the initial
29 stage of the reaction. However, after 15 min, many small puncta with diameters of less than 1 μm
30 emerged. These puncta exhibited Brownian movement and gradually grew into larger distorted
31 vesicle-like assemblies with diameters of 3–5 μm (they resembled ring-like structures in *xy* slice
32 images: see Fig. 2c and Supplementary Fig. 4 for a *z*-stack 3D image). The membrane comprised
33 two thin-layer structures that thermally fluctuated, as confirmed by line plot analysis

1 (Supplementary Fig. 5). These vesicle-like assemblies increased in size (typically to more than 10
2 μm in diameter), mainly by fusing with each other, then transformed into coacervate droplets via
3 unique dynamic structural changes. As shown in Fig. 2d, three small vesicle-like assemblies
4 (diameters: 3, 3.5, and 5 μm) touched each other to form larger distorted assemblies with several
5 crosslinking points (longest diameter: approximately 10 μm). The resultant assemblies frequently
6 transformed into various shapes with crosslinking points that dynamically engaged and disengaged
7 (indicated by yellow and blue arrows in Fig. 2d, respectively). Subsequently, numerous crosslinking
8 points spontaneously formed at the centers of the self-assemblies, and the swaying outer edge of the
9 membrane was gradually incorporated into the core with forming new crosslinking points, resulting
10 in a distorted spherical assemblage with a complex densely-meshed network (diameter:
11 approximately 6 μm). We term this unique process “membrane folding”, and it ended within
12 approximately 6 min. The mesh network of the spherical assemblies rapidly rearranged, and the
13 assemblies coalesced into larger assemblies. Our observations indicated that the resultant
14 assemblies were liquid-like rather than solid-like, namely coacervates. The control experiments
15 confirmed that neither the vesicle-like intermediates nor the coacervate droplets occurred in the
16 absence of PEG₉-F-OH, H-F-OtBu, or DMT-MM, indicating that they comprised PEG₉-FF-OtBu
17 (Supplementary Fig. 6). We noticed that the observed mesh network resembled the inner self-
18 assembling structure of coacervates previously revealed by cryo-TEM. For the first time, the
19 designed *in situ* generation protocol of the coacervate-forming dipeptide enabled us to observe the
20 formation of a coacervate bearing an inner mesh network by time-lapse Airyscan imaging.

21 Using this simple system, we examined the dependence of coacervate formation on amino
22 acids by utilizing various *t*Bu esters of aromatic, hydrophobic, and hydrophilic amino acids instead
23 of H-F-OtBu (H-W-OtBu, H-L-OtBu, H-S-OtBu, and H-G-OtBu; each compound is abbreviated
24 using the single-letter amino acid designation, Fig. 2a). Time-lapse Airyscan imaging revealed that
25 numerous liquid-like coacervate droplets emerged when using W and L (FW and FL core
26 generation, respectively, Fig. 3a, 3b, Supplementary Movie 2, Supplementary Movie 3). In these
27 cases, small μm -sized droplets initially appeared, then increased in size through growth and/or
28 fusion processes (Supplementary Fig. 7a, 7b). In contrast, in the cases of S and G (FS and FG core
29 generation, respectively), a very small number of irregularly shaped aggregates appeared, indicating
30 that the hydrophobic dipeptide core is essential for coacervate formation (Fig. 3c, 3d,
31 Supplementary Fig. 7c, 7d). RP-HPLC analysis confirmed the formation of the desired dipeptide
32 derivatives in all cases (Supplementary Fig. 8). Fluorescence intensity analysis of the entire field of
33 view revealed distinct initiation of coacervate formation times of approximately 40 min for F and W

1 and approximately 75 min for L (Fig. 3e). To understand the coacervate formation steps in detail,
2 we also analyzed the time course changes of the cross-sectional areas at single-droplet resolution, as
3 shown in Fig. 3f and 3g. In the case of L, a gradual area increment was observed in addition to a
4 stepwise increment, revealing that these droplets grew through both dipeptide uptake and fusion
5 (Fig. 3g, Supplementary Fig. 9b). In sharp contrast, the droplet size remained almost constant and
6 increased stochastically in a stepwise manner in the case of W, indicating that coacervate growth
7 proceeded mainly through fusion but not uptake of the dipeptide into droplets (Fig. 3f,
8 Supplementary Fig. 9a). Moreover, we found that some of the droplets shrank, that is the coacervate
9 areas gradually decreased over time (as indicated by the red and purple lines in Fig. 3f). As shown
10 in Fig. 3h, the shrinkage occurred in droplets when another droplet was nearby. Droplet **1** had an
11 area of $13 \mu\text{m}^2$ at 1 h 15 min; it gradually decreased to $5.0 \mu\text{m}^2$ at 2 h, whereas droplet **2** located
12 next to droplet **1** gradually increased from 26 to $33 \mu\text{m}^2$. Time-lapse imaging suggests that a
13 coacervate-forming dipeptide may have been transferred from droplet **1** to droplet **2**. It is worth
14 noting that the vesicle-like intermediates were never observed in any of the cases except for the FF
15 core. All the coacervate formations we examined were initiated through nucleation, but the growth
16 processes were diverse depending on the amino acid sequence.

17

18 **Detailed examination of the PEG₉-FF-OtBu coacervate structure**

19 We subsequently confirmed that the same coacervates were formed using pure PEG₉-FF-OtBu
20 separately synthesized in batches. The coacervate droplets were prepared by adding a buffer to
21 PEG₉-FF-OtBu, then ultrasonicated and thermally annealing to obtain a white suspension
22 (Supplementary Fig. 10, see Methods for detail). Widefield microscopic examination of the
23 resultant suspension revealed micrometer-sized droplets that fused with each other (Supplementary
24 Fig. 11). According to microrheological analysis using the Stokes–Einstein equation, the inner
25 viscosity of the coacervate was approximately $3.68 \pm 0.18 \text{ Pa}\cdot\text{s}$ (the value was similar to the values
26 of other polymer- and protein-based coacervate droplets^{34,40}) (Supplementary Fig. 12). We also
27 determined that the critical coacervation concentration was 0.3 mM (Supplementary Fig. 10). These
28 data revealed that the PEG₉-FF-OtBu formed a liquid-like coacervate.

29 To investigate the structures and properties of coacervate droplets in detail, we next visualized
30 the inner 3D structures of coacervate droplets by Airyscan. To determine the localization of PEG₉-
31 FF-OtBu, we employed a fluorescent probe, i.e., BODIPY-FF-OtBu, which comprises a BODIPY
32 dye at the *N*-terminus of the FF-OtBu motif (Fig. 1c). As shown in Fig. 4a, 4b, and Supplementary
33 Movie 4, the coacervate droplets comprised bright, densely-interconnected mesh structures and

1 dark, irregularly shaped and sized voids (pores), which were similar to the structures observed
2 during the *in situ* formation protocol. Line plot analysis revealed the width of the mesh network to
3 be approximately 100–200 nm (Fig. 4c). According to quantitative image analysis, the average size
4 of the voids was $0.03 \pm 0.05 \mu\text{m}^2$ (mean \pm s.d.) (Fig. 4d). The *z*-stacked 3D image revealed that the
5 mesh network was interconnected, even in the *z*-direction, forming a 3D sponge-like bicontinuous
6 structure (Fig. 4e, Supplementary Movie 5). A time-lapse movie revealed that the 3D sponge-like
7 network fluctuated extensively (Supplementary Movie 4). When the images obtained at different
8 time-points (25.02 and 25.92 s) were overlaid, the networks seemed similar but did not completely
9 overlap with each other (Supplementary Fig. 13, Supplementary Movie 6). We carried out
10 fluorescence recovery after photobleaching (FRAP) analysis using BODIPY-FF-OtBu as a probe to
11 investigate molecular diffusion inside the sponge-like network. After photobleaching, the
12 fluorescence intensity gradually recovered from the outer edge of the photobleached region over 15
13 s (Fig. 4f, Supplementary Fig. 14a, Supplementary Movie 7). According to exponential fitting
14 analysis, the mobile fraction was $89\% \pm 3\%$ and the half recovery time was 2.4 ± 0.2 s
15 (Supplementary Fig. 14b–d). Considering these data and the hydrophobicity of BODIPY-FF-OtBu,
16 the fluorescence probe was able to diffuse within the network. To investigate the chemical
17 properties of the sponge-like network, we determined the uptake of two chemically distinct
18 fluorescent dyes, i.e., fluorescein and rho6G (Supplementary Fig. 1). The microscope images
19 revealed that hydrophobic rho6G was sequestered in the network, but hydrophilic fluorescein was
20 not concentrated inside the coacervate (Supplementary Fig. 15). These uptake behaviors were
21 consistent with the results from quantitative fluorescent spectroscopy analysis (Supplementary Fig.
22 16); the uptake tendency differed from that of the cationic PhePy-FF-OtBu coacervate
23 (Supplementary Fig. 16c).³⁴ Therefore, it seems that the sponge-like network provides a
24 hydrophobic environment comprising the FF-OtBu moiety, and the PEG₉ moiety stabilizes the
25 interface between the mesh and the water/buffer-filled voids.

26

27 **Unique dynamic behavior revealed by real-time imaging**

28 During the real-time imaging experiments, we discovered that the 3D sponge-like coacervate
29 network exhibited dynamic behavior. First, the crosslinks in the network repeatedly engaged and
30 disengaged on a timescale of several tens of milliseconds. We monitored the membrane fluctuation
31 of the coacervate at high spatiotemporal resolution using the Airyscan multiplex mode (16.7 frames
32 per second). As shown in Fig. 4g and Supplementary Movie 6, the outer and inner membranes were
33 connected to each other to form a crosslinking point until 25.26 s (indicated by the white arrow).

1 The crosslinking point was then cleaved from 25.50 to 26.28 s, followed by recovery after 26.52 s.
2 The stochastic engagement and disengagement of the coacervate crosslinks contrast with the static
3 crosslinks of hydrogels, and reflect the liquid-like behavior of coacervates.

4 Such dynamic behavior of the coacervate crosslinks plays an important role in the fusion
5 process. Indeed, real-time imaging of the fusion process revealed a unique “kissing” event before
6 fusion. Fig. 4h and Supplementary Movie 8 show that the outer membranes of distinct coacervate
7 droplets touched each other at 32 s but they disengaged at 34 s, suggesting that this temporal kissing
8 of the coacervate membrane did not induce fusion. From 1 min 30 s, the same coacervate droplets
9 touched several times (Fig. 4h, 4i). At 1 min 40 s, the touching area increased, and then the two
10 coacervate droplets started to fuse with each other. Immediately after the fusion process started, the
11 inner mesh structures of the two droplets interacted and mixed. It is clear that the coacervate fusion
12 started stochastically through such temporal contact between the outer mesh structures.

13

14 **Pathway-dependent thermally responsive phase transition of the coacervate**

15 The inner structure of a coacervate differs depending on the observation temperature (Fig. 5a). It is
16 well known that polymers modified with PEG chains exhibit thermally responsive phase transition
17 through dehydration of the PEG moiety during heating at a critical temperature (the so-called lower
18 critical solution temperature, LCST).^{26,41} We made microscopic observations in the higher
19 temperature (HT) phase at 37 °C. Airyscan imaging revealed spherical assemblies with diameters of
20 several μm that exhibited coalescence (Fig. 5b, Supplementary Fig. 17). Notably, the 3D sponge-
21 like structure observed at 25 °C (the lower temperature (LT) phase) was not visible during the HT
22 phase. FRAP and microrheological analysis revealed liquid-like properties, indicating that PEG₉-
23 FF-OtBu forms a coacervate even in the HT phase (Supplementary Fig. 14 and 12, respectively).
24 Quantitative analysis revealed differences in the coacervate structures between the HT and LT
25 phases. Line plot analysis confirmed that the fluorescence intensity in a single droplet was almost
26 constant during the HT phase (0.96 ± 0.02 ; Fig. 5c red, Supplementary Fig. 18), whereas the
27 intensity varied markedly during the LT phase owing to the 3D sponge-like network structure (0.77
28 ± 0.09 ; Fig. 5c blue, Supplementary Fig. 18). We also noticed that the coacervate shape near a glass
29 surface seemed almost spherical during the HT phase but was highly distorted during the LT phase;
30 the circularity during the HT phase was estimated to be close to one (0.907 ± 0.008), whereas that
31 during the LT phase was 0.70 ± 0.08 (Supplementary Fig. 19). Furthermore, the coalescence
32 kinetics during the HT phase were much faster than during the LT phase (Supplementary Fig. 11,
33 17). These data suggest that the interfacial tension during the HT phase may be higher than during

1 the LT phase. A solution of a coacervate with a shorter diethylene glycol-tethered dipeptide
2 derivative (PEG₂-FF-OtBu) did not exhibit the temperature-dependent structural change
3 (Supplementary Fig. 20, 21). Therefore, the PEG₉-FF-OtBu exhibited a coacervate-to-coacervate
4 transition in response to temperature change.

5 We subsequently attempted *in situ* time-lapse imaging of the thermally responsive coacervate-
6 to-coacervate transition in detail. First, we observed the structural transformation from the LT phase
7 to the HT phase induced by heating (Fig. 5d, Supplementary Movie 9; the sample appears to move
8 because the focus plane drifted owing to the temperature change). After 3 min, the thin-layer
9 membrane structures budded at the periphery of the coacervate (width: approximately 250–300 nm,
10 Fig. 5e, 5f, Supplementary Fig. 22). Concurrently, the darker regions stochastically appeared inside
11 the coacervate. During incubation at 37 °C, the inner darker regions grew and fused with each other,
12 and ultimately moved to the edge of the coacervate droplet. Simultaneously, the inner structure
13 became homogeneous and the fluorescence intensity of the coacervate phase increased, probably
14 owing to an increment of quantum yield (Supplementary Fig. 23). This phase transition behavior
15 proceeded rapidly (within 5 min). After further incubation, the membranes suddenly burst
16 producing numerous spherical coacervates. It was not possible to stain the interiors of the budded
17 thin-layer membranes and inner-separated regions with BODIPY-FF-OtBu, suggesting that their
18 interiors were filled with water/buffer (thus, the inner darker regions can be ascribed to
19 vacuoles^{16,33,42–44}). Temperature-dependent phase transition was also confirmed in the bulk state
20 (Supplementary Fig. 10, 24). Given the temperature-responsive dehydration of the PEG chain, it is
21 reasonable to suppose that the formation of the budded membranes and the inner vacuoles was
22 induced by phase separation due to water release from the PEG₉ chain.

23 Interestingly, the phase transition from the HT to the LT phase proceeded through a different
24 intermediate state (Fig. 5g, Supplementary Movie 10). After setting the temperature controller to
25 cool from 37 to 25 °C, the coacervate droplets coalesced and the fluorescence intensity gradually
26 and simultaneously decreased. After 30 min, the inner sponge-like network appeared without the
27 budded membranes and the dark vacuoles inside the coacervates. The overall changes were
28 completed within approximately 60 min. Compared with the LT-to-HT phase transition, the HT-to-
29 LT phase took much longer to reach a thermally equilibrated state, probably because of slow
30 water/buffer uptake into the coacervate droplets for the hydration of the PEG₉ chain. This may have
31 been the main reason the PEG₉-FF-OtBu coacervates exhibited pathway-dependent phase transition
32 behavior.

33

1 **Photo-induced transient phase separation inside a coacervate containing gold nanoparticles**
2 Encouraged by the temperature-responsive coacervate-to-coacervate transition, we manipulated the
3 inner structure of a coacervate by exploiting the photothermal effect of gold nanoparticles
4 (AuNPs).^{12,45} It is reasonable to suppose that thermally induced coacervate-to-coacervate transition
5 can be triggered by local heat generation induced by irradiating AuNPs trapped in the coacervate
6 with light (Fig. 6a). A solution containing AuNPs with diameters of 100 nm was added to the
7 coacervate solution, and the resultant mixture was incubated at 37 °C for 15 min, then at 25 °C for 1
8 h. A widefield microscope image revealed that the AuNPs were entrapped inside the coacervate
9 (Fig. 6b). We then locally irradiated the entrapped AuNPs for 7.3 s with intense laser light (561 nm)
10 using a FRAP experiment setup, and monitored time-dependent changes. Immediately after light
11 irradiation, a higher fluorescence region with a diameter of approximately 4 μm appeared around
12 the irradiated region (Fig. 6c, 6d, Supplementary Movie 11). The 3D sponge-like structure was not
13 visible in this region, so the higher fluorescence region can be assigned to the HT phase.
14 Subsequently, the HT phase region gradually broadened and the boundary between the LT phase
15 became unclear. After approximately 70 s, the HT phase region completely disappeared.
16 Concurrently, thin layer-like membranes similar to those observed during the LT-to-HT phase
17 transition budded at the periphery of the coacervate, suggesting that water/buffer was expelled from
18 the temporal HT region owing to dehydration of the PEG₉ chain. According to the quantitative
19 analysis of the fluorescence intensity, the half-life of the temporal HT region was approximately
20 26.0 ± 0.4 s (Fig. 6e). The coacervate diameter transiently decreased immediately after laser
21 irradiation, and started to increase after 40 s (Fig. 6f). A control experiment confirmed that such
22 local phase separation did not occur when the AuNPs-free area was irradiated with 561 nm laser
23 radiation (Supplementary Fig. 25). These results indicate that the structures and properties of a
24 PEG₉-FF-OtBu coacervate can be spatiotemporally controlled by combining it with functional
25 nanoparticles.

26

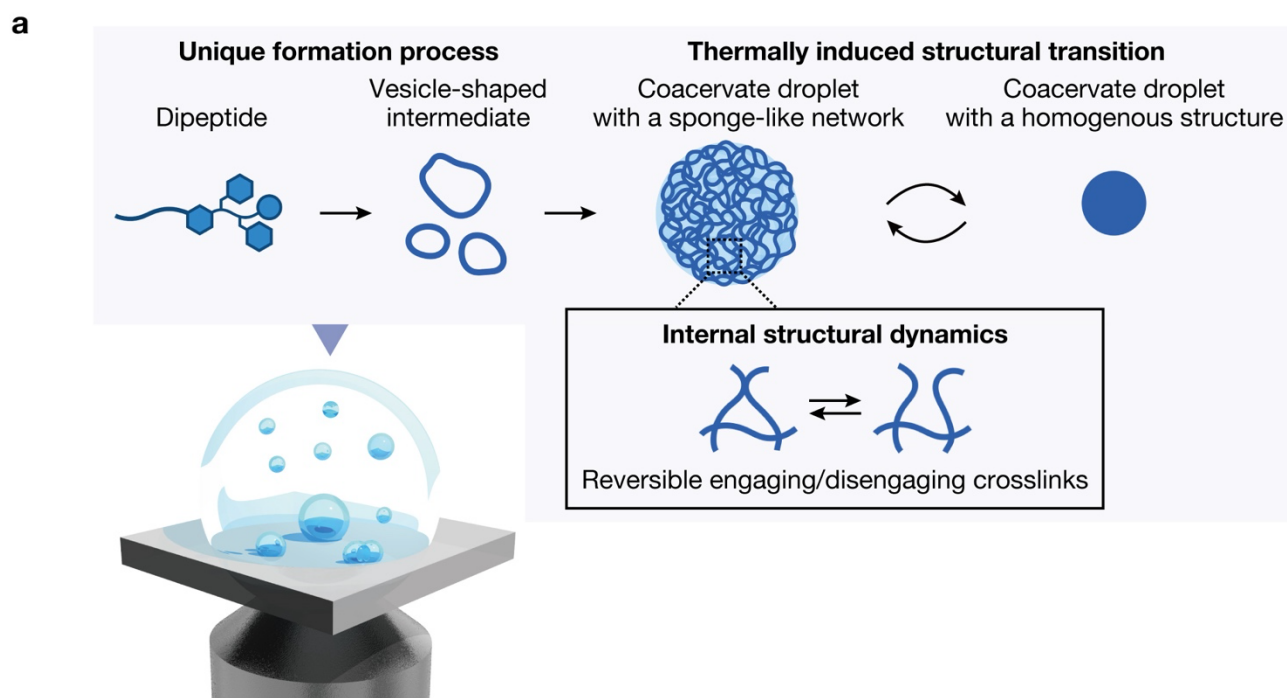
27 **Discussion**

28 The results presented herein demonstrate that 3D sponge-like inner/interfacial networks are
29 remarkably dynamic in coacervate droplets. Although cryo-TEM/SEM have been used to
30 characterized sponge-like networks as the inner self-assembling structures of coacervates, these
31 EM-based observation techniques can only provide static structural information owing to sample
32 freezing and/or fixation. Even using the rapidly developing liquid phase TEM technique,
33 researchers have not been able to obtain clear images of the sponge-like coacervate network in real

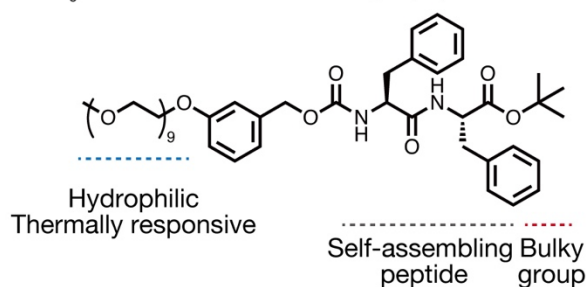
1 time.⁴⁶ Therefore, investigations of the inner dynamics of coacervates rely heavily on FRAP and/or
2 fluorescence correlation spectroscopy (FCS) analyses, which only provide the diffusion coefficients
3 of fluorescently labeled components. In contrast, our real-time imaging study revealed various types
4 of fluctuation of the sponge-like network, including reversible crosslinking formation and stochastic
5 membrane kissing. Moreover, we succeeded in observing the formation of these 3D sponge-like
6 networks, which involves an unprecedented membrane folding step of the intermediate vesicle-
7 shaped assemblies. This observation is consistent with an earlier report on the structural
8 transformation from a shear-induced metastable L_{α} phase (multilamellar) to a thermally equilibrated
9 L_3 phase (coacervate) confirmed by a single snapshot obtained using freeze fracture EM.²³ Our
10 results provide a better understanding of the structure–property relationships of coacervates, and
11 deliver valuable insights into both synthetic and biological LLPS, whose formation mechanism
12 remains poorly understood.

13 We also achieved the photo-induced generation of a multiphase coacervate using encapsulated
14 AuNPs. Multiphase coacervates have received considerable attention because they are involved in
15 myriad essential biological processes.⁴⁷ Inspired by these biological events, a few synthetic
16 multiphase LLPS materials have been developed by careful combination of different coacervates
17 with distinct physicochemical properties (e.g., interfacial tension).^{34,42,48–50} However, transient
18 multiphase coacervation is carried out in a different manner, i.e., the *in situ* generation of distinct
19 coacervate phases consisting of a single dipeptide derivative by integration of its thermally induced
20 response and the photothermal effect of AuNPs. Such stimulus-triggered control of the sponge-like
21 network in terms of mesh size and dynamics could provide a new way of manipulating the liquid-
22 like properties of synthetic and biological LLPS materials. Our droplet engineering will facilitate
23 the development of evolvable artificial cells by controlled growth and division, and enable
24 condensate-targeted drug development by inhibiting neurodegenerative aggregation in the near
25 future.

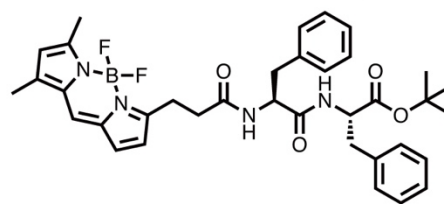
26



b PEG₉-FF-OtBu: self-assembling dipeptide for LLPS

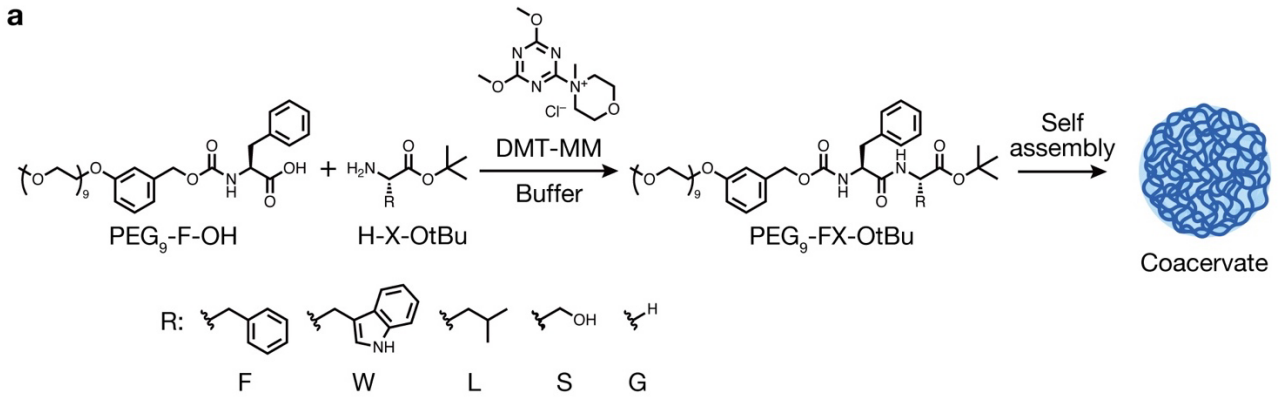


c BODIPY-FF-OtBu: fluorescent probe

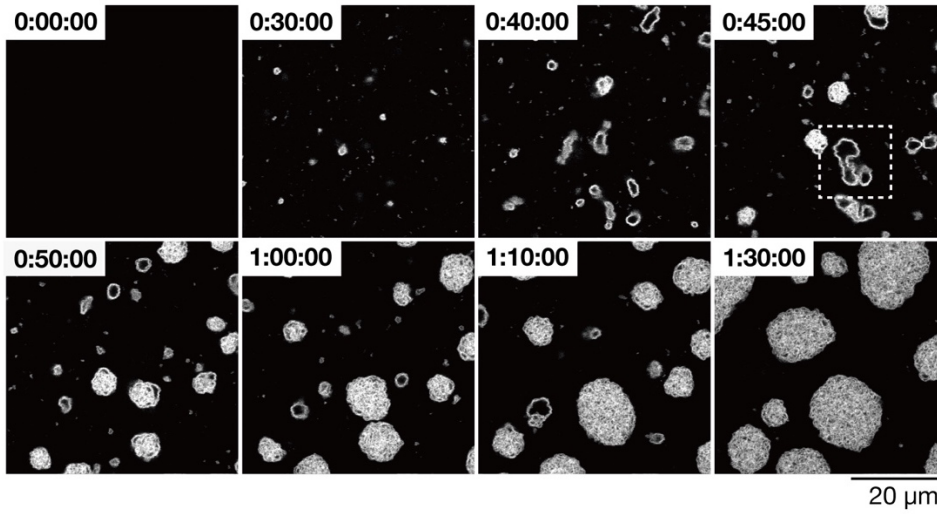


1
2
3
4
5
6
7

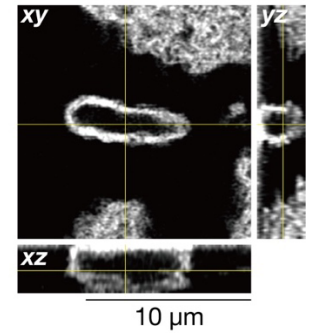
Fig. 1. Conceptual illustration of this research. (a) Schematic illustration of real-time confocal imaging of formation and dynamics of a three-dimensional (3D) sponge-like network in a dipeptide-based coacervate. (b,c) Chemical structures of (b) a self-assembling dipeptide derivative for liquid-liquid phase separation (LLPS), PEG₉-FF-OtBu, and (c) a fluorescent probe, BODIPY-FF-OtBu. Other molecules used in this study are shown in Supplementary Fig. 1.



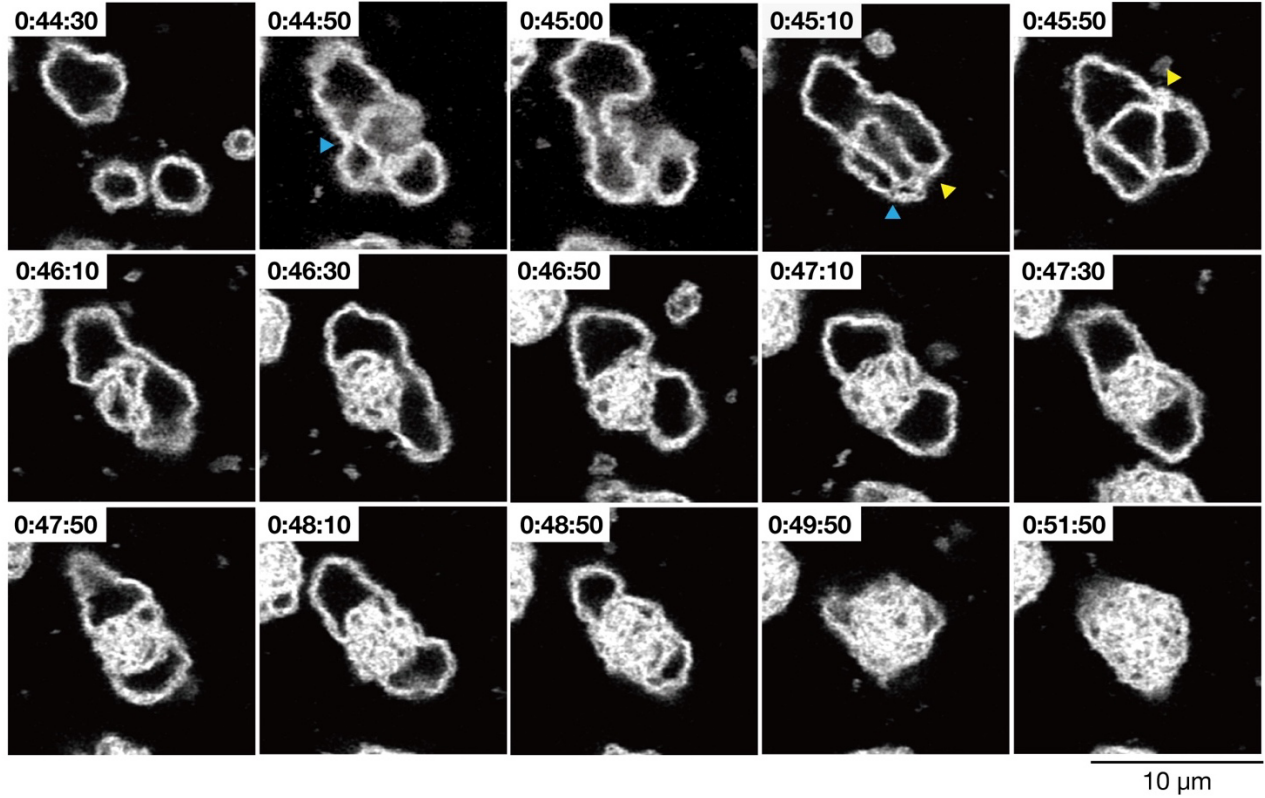
b H-F-OtBu, Time: h:mm:ss



c H-F-OtBu



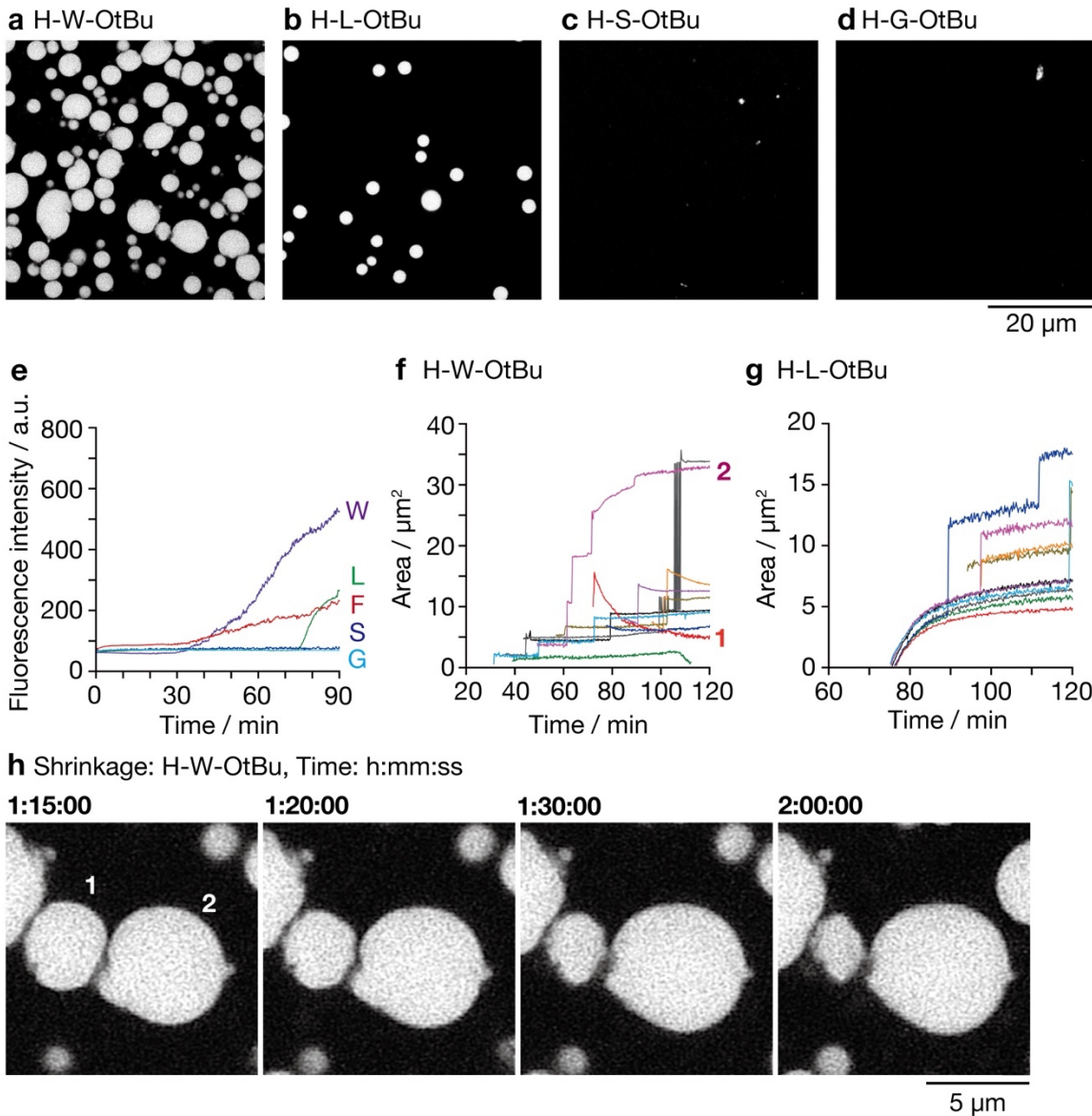
d H-F-OtBu, Time: h:mm:ss



1
2

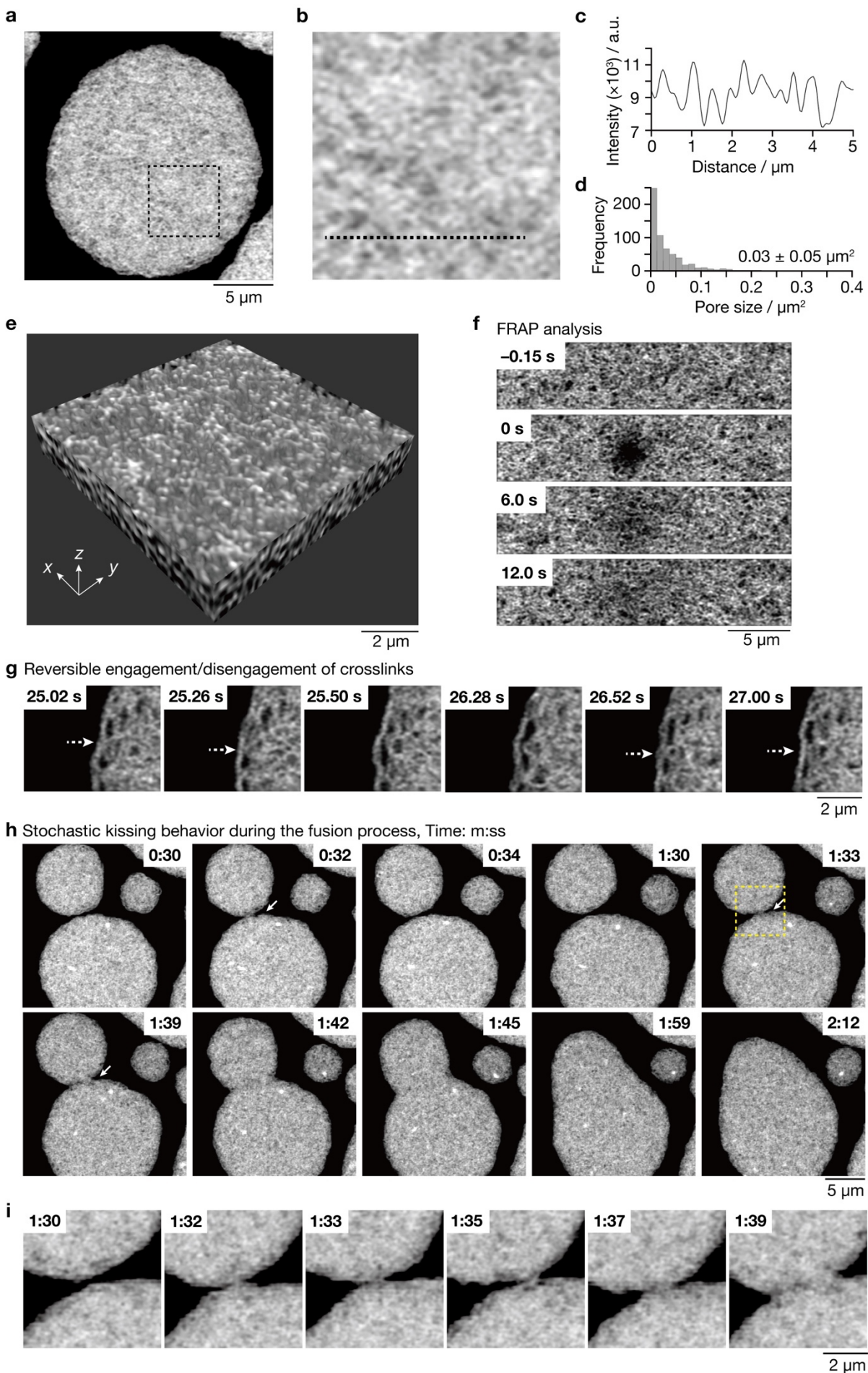
1 **Fig. 2. Real-time Airyscan imaging of formation of the 3D sponge-like network.** (a) Scheme for
2 a reaction for *in situ* generation of the dipeptide derivatives by condensation between PEG₉-F-OH
3 and H-X-OtBu in the presence of DMT-MM. (b) Real-time confocal images of the formation
4 process of PEG₉-FF-OtBu coacervates. (c) 3D imaging of an intermediate vesicle-like assembly. (d)
5 Magnified images of the fusion and membrane folding process of vesicle-like assemblies into a
6 coacervate droplet. Blue and yellow arrows highlight points of crosslink cleavage and formation,
7 respectively. Condition: [PEG₉-F-OH] = [H-F-OtBu] = [DMT-MM] = 10 mM, [rhodamine 6G] = 10
8 μM, 50 mM MES, pH 7.0, 25 °C. DMT-MM: 4-(4,6-Dimethoxy-1,3,5-triazin-2-yl)-4-
9 methylmorpholinium chloride.

10

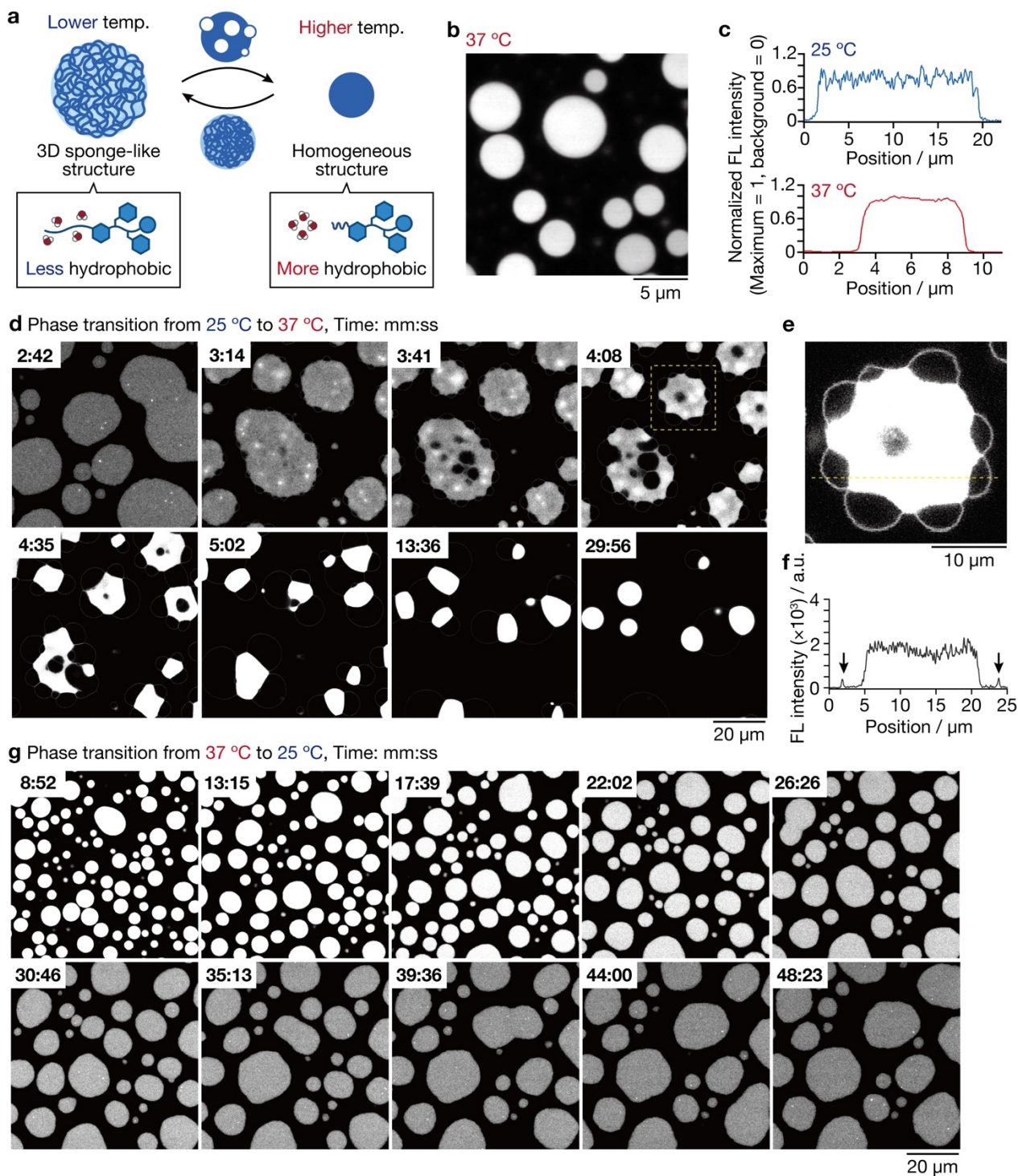


1
2 **Fig. 3. Dependence of coacervate formation on the dipeptide core.** (a–d) Airyscan images 1.5 h
3 after reaction of PEG₉-F-OH and (a) H-W-OtBu, (b) H-L-OtBu, (c) H-S-OtBu, or (d) H-G-OtBu in
4 the presence of DMT-MM. (e) Time course of fluorescence intensity changes during reaction of
5 PEG₉-F-OH and (red) H-F-OtBu, (purple) H-W-OtBu, (green) H-L-OtBu, (blue) H-S-OtBu, or
6 (light blue) H-G-OtBu. (f,g) Time course changes of cross-sectional areas during reaction of PEG₉-
7 F-OH and (f) H-W-OtBu and (g) H-L-OtBu ($n = 10$). Regions of interest are shown in
8 Supplementary Fig. 9. (h) Shrinkage of coacervate droplets when using H-W-OtBu. Condition:
9 [PEG₉-F-OH] = [H-X-OtBu] = [DMT-MM] = 10 mM, [rhodamine 6G] = 10 μM , 50 mM MES, pH
10 7.0, 25 °C.

11
12
13



1 **Fig. 4. Structure and dynamics of the sponge-like network in the coacervate.** (a) Airyscan
2 image of a PEG₉-FF-OtBu coacervate. (b) Magnified image of a black square shown in Fig. 4a. (c)
3 Line plot analysis of fluorescence intensity along a black line shown in Fig. 4b. (d) Distribution of
4 the estimated pore size in the coacervate ($n = 750$). (e) 3D Airyscan image of a PEG₉-FF-OtBu
5 coacervate. A partial structure was shown. (f) Time-lapse images of FRAP analysis. (g) Reversible
6 crosslink engagement and disengagement in the sponge-like network. Crosslinking points are
7 highlighted by white arrows. (h) Stochastic kissing behavior during a coacervate fusion process.
8 Kissing points are highlighted by white arrows. (i) Magnified images of the fusion process,
9 highlighted by a yellow square in Fig. 4h. Condition: [PEG₉-FF-OtBu] = 1.0 mM, [BODIPY-FF-
10 OtBu] = 10 μ M, 50 mM MES, pH 7.0, 25 $^{\circ}$ C.
11



1

2 **Fig. 5. Pathway-dependent thermally responsive phase transition of the coacervate. (a)**
 3 Schematic illustration of thermally responsive phase transition of the PEG₉-FF-OtBu coacervate.
 4 **(b)** Airyscan image of PEG₉-FF-OtBu coacervates at 37 °C. **(c)** Line plot analysis of the normalized
 5 fluorescence intensity at (top) 25 and (bottom) 37 °C. Regions of interest are shown in
 6 Supplementary Fig. 18. **(d,g)** Time-lapse imaging of thermally responsive structural changes of the
 7 coacervates **(d)** from 25 to 37 °C and **(g)** from 37 to 25 °C. **(e)** The magnified image of a budding
 8 coacervate highlighted by a yellow square in Fig. 5d. The contrast is enhanced to highlight thin-

1 layer membrane structures. (f) Line plot analysis of fluorescence (FL) intensity along a yellow line
2 shown in Fig. 5e. Black arrows highlight fluorescence intensity of thin-layer membranes. The
3 temperature dependent phase transition was also examined at the bulk state (Supplementary Fig. 10,
4 24). Condition: [PEG₉-FF-OtBu] = 1.0 mM, [BODIPY-FF-OtBu] = 10 μM, 50 mM MES, pH 7.0,
5 25 or 37 °C.

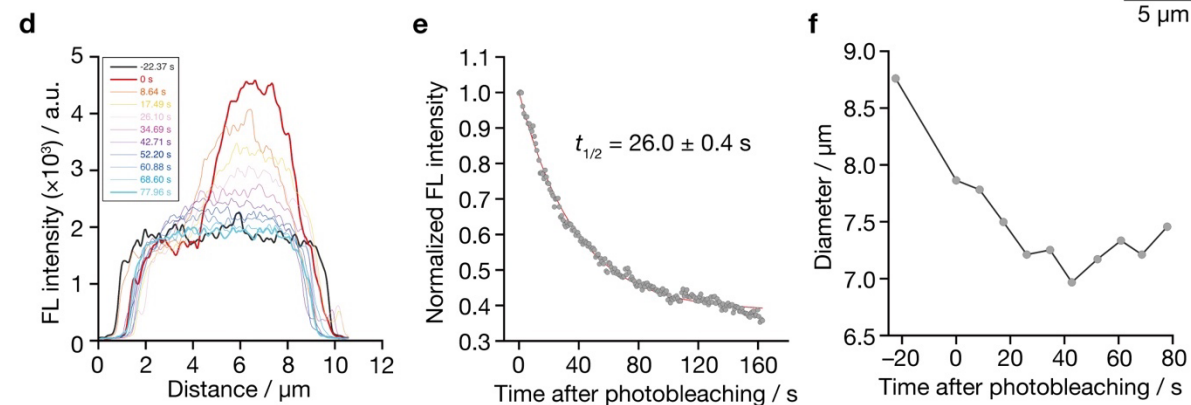
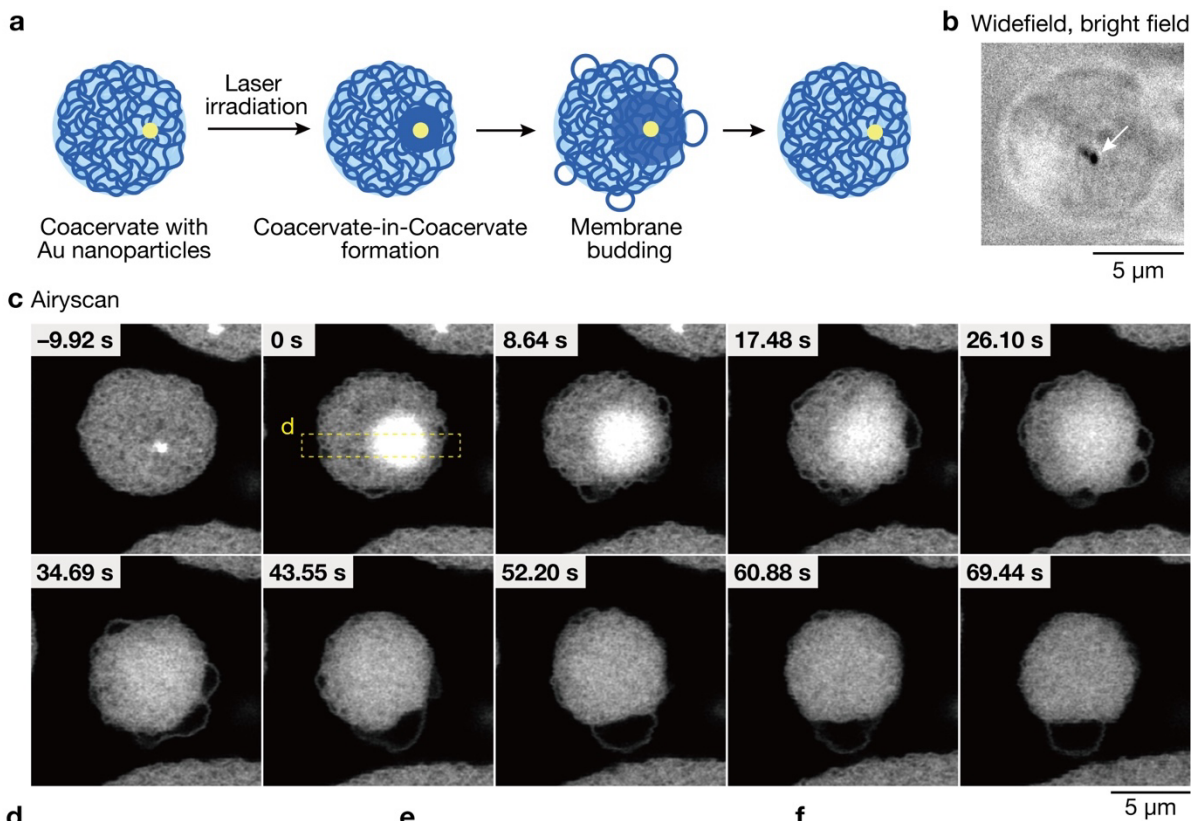


Fig. 6. Photo-induced transient generation of a multiphase coacervate containing gold

nanoparticles (AuNPs). (a) Schematic illustration of photo-induced coacervate manipulation using

AuNPs. (b) Widefield microscopic image of a coacervate containing AuNPs (highlighted by a white

arrow). (c) Time-lapse Airyscan imaging of a coacervate containing AuNPs before and after laser

irradiation. Time just after laser irradiation set at 0 s. (d) Line plot analysis of fluorescence intensity

along a yellow rectangle shown in Fig. 6c. (e,f) Time course changes of (e) fluorescence intensity of

the irradiated area and (f) the coacervate diameter before and after laser irradiation. Condition:

[PEG₉-FF-OtBu] = 1.0 mM, [BODIPY-FF-OtBu] = 10 μM, 50 mM MES, pH 7.0, 25 °C.

1 **Author information**

2 **Corresponding authors**

3 **Ryou Kubota** – *Department of Synthetic Chemistry and Biological Chemistry, Graduate School of*
4 *Engineering, Kyoto University, Katsura, Nishikyo-ku, Kyoto 615-8510, Japan; [orcid.org/0000-](https://orcid.org/0000-0001-8112-8169)*
5 *[0001-8112-8169](https://orcid.org/0001-8112-8169); Email: rkubota@sbchem.kyoto-u.ac.jp*

6 **Itaru Hamachi** – *Department of Synthetic Chemistry and Biological Chemistry, Graduate School*
7 *of Engineering, Kyoto University, Katsura, Nishikyo-ku, Kyoto 615-8510, Japan; JST-ERATO,*
8 *Hamachi Innovative Molecular Technology for Neuroscience, Nishikyo-ku, Kyoto 615-8530, Japan;*
9 *orcid.org/0000-0002-3327-3916; Email: ihamachi@sbchem.kyoto-u.ac.jp*

10

11 **Author**

12 **Taro Hiroi** – *Department of Synthetic Chemistry and Biological Chemistry, Graduate School of*
13 *Engineering, Kyoto University, Katsura, Nishikyo-ku, Kyoto 615-8510, Japan*

14 **Yuchong Liu** – *Department of Synthetic Chemistry and Biological Chemistry, Graduate School of*
15 *Engineering, Kyoto University, Katsura, Nishikyo-ku, Kyoto 615-8510, Japan*

16

17 **Author contribution**

18 R.K. and I.H. designed the work. R.K. conducted all of the experiments and analyzed the data. T.H.
19 found temperature-dependent phase transition of the coacervate. Y.L. synthesized PEG₉- and PEG₂-
20 FF-OtBu. R.K. and I.H. wrote the manuscript.

21

22 **Acknowledgements**

23 We appreciate Dr. Fumiyoshi Ishidate (iCeMS Analysis Center, Kyoto University) for fruitful
24 discussion about Airyscan imaging. This work was supported by a Grant-in-Aid for Scientific
25 Research on Innovative Areas “Chemistry for Multimolecular Crowding Biosystems” (JSPS
26 KAKENHI Grant JP17H06348), the Japan Science and Technology Agency (JST) ERATO Grant
27 Number JPMJER1802 to I.H., and by a Grant-in-Aid for Young Scientists (JSPS KAKENHI Grant
28 JP20K15400) and a Grant-in-Aid for Scientific Research (B) (JSPS KAKENHI Grant JP22H02195)
29 to R.K. We thank Frank Kitching, MSc., from Edanz (<https://jp.edanz.com/ac>) for editing a draft of
30 this manuscript.

31

32 **Competing interests**

33 The authors declare no competing interests.

1 **References**

- 2 1. Shin, Y. & Brangwynne, C. P. Liquid phase condensation in cell physiology and disease.
3 *Science* **357**, eaaf4382 (2017).
- 4 2. Aumiller, W. M., Jr & Keating, C. D. Experimental models for dynamic compartmentalization
5 of biomolecules in liquid organelles: Reversible formation and partitioning in aqueous biphasic
6 systems. *Adv. Colloid Interface Sci.* **239**, 75–87 (2017).
- 7 3. Abbas, M., Lipiński, W. P., Wang, J. & Spruijt, E. Peptide-based coacervates as biomimetic
8 protocells. *Chem. Soc. Rev.* **50**, 3690–3705 (2021).
- 9 4. Abbas, M., Lipiński, W. P., Nakashima, K. K., Huck, W. T. S. & Spruijt, E. A short peptide
10 synthon for liquid-liquid phase separation. *Nat. Chem.* **13**, 1046–1054 (2021).
- 11 5. Tang, Y. *et al.* Prediction and characterization of liquid-liquid phase separation of minimalistic
12 peptides. *Cell Rep. Phys. Sci.* **2**, 100579 (2021).
- 13 6. Niu, J., Qiu, C., Abbott, N. L. & Gellman, S. H. Formation of versus recruitment to RNA-rich
14 condensates: controlling effects exerted by peptide side chain identity. *J. Am. Chem. Soc.* **144**,
15 10386–10395 (2022).
- 16 7. Deepankumar, K. *et al.* Liquid-liquid phase separation of the green mussel adhesive protein
17 Pvfp-5 is regulated by the post-translated dopa amino acid. *Adv. Mater.* **34**, e2103828 (2022).
- 18 8. Jain, A. *et al.* Connected peptide modules enable controlled co-existence of self-assembled
19 fibers inside liquid condensates. *J. Am. Chem. Soc.* **144**, 15002–15007 (2022).
- 20 9. Oparin, A. I. Evolution of the concepts of the origin of life. *Orig. Life* **7**, 3–8 (1976).
- 21 10. Slootbeek, A. D., van Haren, M. H. I., Smokers, I. B. A. & Spruijt, E. Growth, replication and
22 division enable evolution of coacervate protocells. *Chem. Commun.* **58**, 11183–11200 (2022).
- 23 11. Cook, A. B., Novosedlik, S. & van Hest, J. C. M. Complex coacervate materials as artificial
24 cells. *Acc. Mater. Res.* (2023) doi:10.1021/accountsmr.2c00239.
- 25 12. Koga, S., Williams, D. S., Perriman, A. W. & Mann, S. Peptide-nucleotide microdroplets as a
26 step towards a membrane-free protocell model. *Nat. Chem.* **3**, 720–724 (2011).
- 27 13. Dora Tang, T.-Y. *et al.* Fatty acid membrane assembly on coacervate microdroplets as a step
28 towards a hybrid protocell model. *Nat. Chem.* **6**, 527–533 (2014).
- 29 14. Aumiller, W. M., Jr & Keating, C. D. Phosphorylation-mediated RNA/peptide complex
30 coacervation as a model for intracellular liquid organelles. *Nat. Chem.* **8**, 129–137 (2016).
- 31 15. Mason, A. F., Buddingh', B. C., Williams, D. S. & van Hest, J. C. M. Hierarchical self-
32 assembly of a copolymer-stabilized coacervate protocell. *J. Am. Chem. Soc.* **139**, 17309–17312
33 (2017).

- 1 16. Donau, C. *et al.* Active coacervate droplets as a model for membraneless organelles and
2 protocells. *Nat. Commun.* **11**, 5167 (2020).
- 3 17. Matsuo, M. & Kurihara, K. Proliferating coacervate droplets as the missing link between
4 chemistry and biology in the origins of life. *Nat. Commun.* **12**, 5487 (2021).
- 5 18. Xu, C., Martin, N., Li, M. & Mann, S. Living material assembly of bacteriogenic protocells.
6 *Nature* **609**, 1029–1037 (2022).
- 7 19. Ianeselli, A. *et al.* Non-equilibrium conditions inside rock pores drive fission, maintenance and
8 selection of coacervate protocells. *Nat. Chem.* **14**, 32–39 (2022).
- 9 20. Alberti, S. & Hyman, A. A. Biomolecular condensates at the nexus of cellular stress, protein
10 aggregation disease and ageing. *Nat. Rev. Mol. Cell Biol.* **22**, 196–213 (2021).
- 11 21. Jho, Y., Yoo, H. Y., Lin, Y., Han, S. & Hwang, D. S. Molecular and structural basis of low
12 interfacial energy of complex coacervates in water. *Adv. Colloid Interface Sci.* **239**, 61–73
13 (2017).
- 14 22. Strey, R., Jahn, W., Porte, G. & Bassereau, P. Freeze fracture electron microscopy of dilute
15 lamellar and anomalous isotropic (L₃) phases. *Langmuir* **6**, 1635–1639 (1990).
- 16 23. Hoffmann, H., Thunig, C., Munkert, U., Meyer, H. W. & Richter, W. From vesicles to the L₃
17 (sponge) phase in alkyltrimethylamine oxide/heptanol systems. *Langmuir* **8**, 2629–2638
18 (1992).
- 19 24. Menger, F. M., Peresykin, A. V., Caran, K. L. & Apkarian, R. P. A Sponge morphology in an
20 elementary coacervate. *Langmuir* **16**, 9113–9116 (2000).
- 21 25. Imura, T., Yanagishita, H. & Kitamoto, D. Coacervate formation from natural glycolipid: one
22 acetyl group on the headgroup triggers coacervate-to-vesicle transition. *J. Am. Chem. Soc.* **126**,
23 10804–10805 (2004).
- 24 26. Wibowo, A. *et al.* Morphology control in water of polyion complex nanoarchitectures of
25 double-hydrophilic charged block copolymers through composition tuning and thermal
26 treatment. *Macromolecules* **47**, 3086–3092 (2014).
- 27 27. Bhattacharya, A. *et al.* Lipid sponge droplets as programmable synthetic organelles. *Proc. Natl.*
28 *Acad. Sci. U. S. A.* **117**, 18206–18215 (2020).
- 29 28. Sing, C. E. & Perry, S. L. Recent progress in the science of complex coacervation. *Soft Matter*
30 **16**, 2885–2914 (2020).
- 31 29. Spruijt, E., Westphal, A. H., Borst, J. W., Cohen Stuart, M. A. & van der Gucht, J. Binodal
32 compositions of polyelectrolyte complexes. *Macromolecules* **43**, 6476–6484 (2010).
- 33 30. Marciel, A. B., Srivastava, S. & Tirrell, M. V. Structure and rheology of polyelectrolyte

- 1 complex coacervates. *Soft Matter* **14**, 2454–2464 (2018).
- 2 31. Kubota, R., Tanaka, W. & Hamachi, I. Microscopic imaging techniques for molecular
3 assemblies: electron, atomic force, and confocal microscopies. *Chem. Rev.* **121**, 14281–14347
4 (2021).
- 5 32. Nakashima, K. K., van Haren, M. H. I., André, A. A. M., Robu, I. & Spruijt, E. Active
6 coacervate droplets are protocells that grow and resist Ostwald ripening. *Nat. Commun.* **12**,
7 3819 (2021).
- 8 33. Bergmann, A. M. *et al.* Evolution and single-droplet analysis of fuel-driven compartments by
9 droplet-based microfluidics. *Angew. Chem. Int. Ed.* **61**, e202203928 (2022).
- 10 34. Kubota, R., Torigoe, S. & Hamachi, I. Temporal stimulus patterns drive differentiation of a
11 synthetic dipeptide-based coacervate. *J. Am. Chem. Soc.* **144**, 15155–15164 (2022).
- 12 35. Sheehan, F. *et al.* Peptide-based supramolecular systems chemistry. *Chem. Rev.* **121**, 13869–
13 13914 (2021).
- 14 36. Reches, M. & Gazit, E. Casting metal nanowires within discrete self-assembled peptide
15 nanotubes. *Science* **300**, 625–627 (2003).
- 16 37. Yang, Z., Liang, G., Wang, L. & Xu, B. Using a kinase/phosphatase switch to regulate a
17 supramolecular hydrogel and forming the supramolecular hydrogel in vivo. *J. Am. Chem. Soc.*
18 **128**, 3038–3043 (2006).
- 19 38. Ikeda, M., Tanida, T., Yoshii, T. & Hamachi, I. Rational molecular design of stimulus-
20 responsive supramolecular hydrogels based on dipeptides. *Adv. Mater.* **23**, 2819–2822 (2011).
- 21 39. Kunishima, M., Kawachi, C., Hioki, K., Terao, K. & Tani, S. Formation of carboxamides by
22 direct condensation of carboxylic acids and amines in alcohols using a new alcohol- and water-
23 soluble condensing agent: DMT-MM. *Tetrahedron* **57**, 1551–1558 (2001).
- 24 40. Folkmann, A. W., Putnam, A., Lee, C. F. & Seydoux, G. Regulation of biomolecular
25 condensates by interfacial protein clusters. *Science* **373**, 1218–1224 (2021).
- 26 41. Saeki, S., Kuwahara, N., Nakata, M. & Kaneko, M. Upper and lower critical solution
27 temperatures in poly (ethylene glycol) solutions. *Polymer* **17**, 685–689 (1976).
- 28 42. Donau, C., Späth, F., Stasi, M., Bergmann, A. M. & Boekhoven, J. Phase transitions in
29 chemically fueled, multiphase complex coacervate droplets. *Angew. Chem. Int. Ed.* **61**,
30 e202211905 (2022).
- 31 43. Alshareedah, I., Moosa, M. M., Raju, M., Potoyan, D. A. & Banerjee, P. R. Phase transition of
32 RNA – protein complexes into ordered hollow condensates. *Proc. Natl. Acad. Sci. U. S. A.* **117**,
33 15650–15658 (2020).

- 1 44. Erkamp, N. A. *et al.* Spatially non-uniform condensates emerge from dynamically arrested
2 phase separation. *Nat. Commun.* **14**, 684 (2023).
- 3 45. Gao, N., Xu, C., Yin, Z., Li, M. & Mann, S. Triggerable protocell capture in nanoparticle-
4 caged coacervate microdroplets. *J. Am. Chem. Soc.* **144**, 3855–3862 (2022).
- 5 46. Le Ferrand, H., Duchamp, M., Gabryelczyk, B., Cai, H. & Miserez, A. Time-resolved
6 observations of liquid-liquid phase separation at the nanoscale using *in situ* liquid transmission
7 electron microscopy. *J. Am. Chem. Soc.* **141**, 7202–7210 (2019).
- 8 47. Feric, M. *et al.* Coexisting liquid phases underlie nucleolar subcompartments. *Cell* **165**, 1686–
9 1697 (2016).
- 10 48. Lu, T. & Spruijt, E. Multiphase complex coacervate droplets. *J. Am. Chem. Soc.* **142**, 2905–
11 2914 (2020).
- 12 49. Karoui, H., Seck, M. J. & Martin, N. Self-programmed enzyme phase separation and
13 multiphase coacervate droplet organization. *Chem. Sci.* **12**, 2794–2802 (2021).
- 14 50. Choi, S., Meyer, M. O., Bevilacqua, P. C. & Keating, C. D. Phase-specific RNA accumulation
15 and duplex thermodynamics in multiphase coacervate models for membraneless organelles.
16 *Nat. Chem.* **14**, 1110–1117 (2022).